Published in final edited form as:

Structure. 2015 December 1; 23(12): 2291–2299. doi:10.1016/j.str.2015.07.024.

The importance of ligand-receptor conformational pairs in stabilization: spotlight on the N/OFQ G protein-coupled receptor

Rebecca L. Miller[1,6], **Aaron A. Thompson**[1,6], **Claudio Trapella**[2], **Remo Guerrini**[2], **Davide Malfacini**[3], **Nilkanth Patel**[5], **Gye Won Han**[4], **Vadim Cherezov**[4], **Girolamo Caló**[3], **Vsevolod Katritch**[5], and **Raymond C. Stevens**[1,4,5,*]

[1]Department of Integrative Structural and Computational Biology, The Scripps Research Institute, La Jolla CA 92037, USA

[2]Department of Chemical and Pharmaceutical Sciences and LTTA (Laboratorio per le Tecnologie delle Terapie Avanzate), University of Ferrara, 44121 Ferrara, Italy

[3]Department of Medical Sciences, Section of Pharmacology and National Institute of Neuroscience, University of Ferrara, 44121 Ferrara, Italy

[4]Department of Chemistry, Bridge Institute, University of Southern California, Los Angeles CA 90089, USA

[5]Department of Biological Sciences, Bridge Institute, University of Southern California, Los Angeles CA 90089, USA

Summary

Understanding the mechanism by which ligands impact receptor conformational equilibria is key in accelerating membrane protein structural biology. In the case of G protein-coupled receptors (GPCRs) we currently pursue a brute force approach for identifying ligands that stabilize receptors and facilitate crystallogenesis. The nociceptin/orphanin FQ peptide receptor (NOP) is a member of the opioid receptor subfamily of GPCRs for which many structurally diverse ligands are available for screening. We observed that antagonist potency is correlated with a ligand's ability to induce

*Correspondence: Raymond C. Stevens (stevens@usc.edu).
[6]These authors contributed equally to this work

Accession Numbers

Coordinates and structure factors for the two crystal structures have been deposited in the RCSB Protein Data Bank under accession codes 5DHH (NOP–SB-612111) and 5DHG (NOP–C35).

Author Contributions

R.L.M. purified and crystallized the receptor in LCP, collected and processed diffraction data, determined and refined the structure, analyzed the data, and wrote the paper. A.A.T. identified the compounds for crystallization, purified and crystallized the receptor in LCP, collected and processed diffraction data, and wrote the paper. C.T. synthesized ligands for structural studies. R.G. and G.C. synthesized ligands for structural studies and wrote the paper. D.M performed the pharmacological experiments and wrote the paper. N.P. and V.K. performed docking studies, analyzed the data, and wrote the paper. V.C. and R.S. were responsible for the overall project strategy and management.

Competing Financial Interests

The authors declare no competing financial interests.

receptor stability (T_m) and crystallogenesis. Using this screening strategy, we solved two structures of NOP in complex with top candidate ligands SB-612111 and C-35. Docking studies indicate that while potent, stabilizing antagonists strongly favor a single binding orientation, less potent ligands can adopt multiple binding modes, contributing to their low T_m values. These results suggest a mechanism for ligand-aided crystallogenesis whereby potent antagonists stabilize a single ligand-receptor conformational pair.

Keywords

Nociceptin/orphanin FQ peptide receptor; NOP; ORL-1; N/OFQ; opioid receptor; G protein-coupled receptor; GPCR; membrane protein; lipidic cubic phase; BRET; receptor-ligand conformational pair

Introduction

G protein-coupled receptors (GPCRs) are intrinsically dynamic cell surface receptors that play many key roles in human physiology and pathology, mediating the action of over 30% of clinically marketed drugs (Rask-Andersen et al., 2014). Structural studies that inform our understanding of GPCR-drug interactions are currently impeded by our lack of understanding surrounding receptor stabilization and its connection to crystallogenesis.

Virtually all of the 31 unique GPCR structures available include ligands that aid in receptor crystallogenesis, with ligand properties such as affinity (pK_i), molecular weight (MW), and lipophilicity (LogP or LogD) impacting the outcome of crystallization trials (Zhang et al., 2015). In a recent survey of ligands from GPCR co-crystal structures, 77% of ligands were found to possess affinities in the single-digit nanomolar (nM) range, 96% of ligands had octanol-water partition coefficients (LogPs) below 5, and 76% had MWs between 200–500 Da (Zhang et al., 2015). As GPCRs are pervasive drug targets, it is not surprising that many ligands that have been developed to target these receptors fall within the well-known Lipinski's "Rule of Five" criteria for drug-like compounds (MW ≤ 500 Da, LogP ≤ 5) (Lipinski, 2004).

The ability of a ligand to increase a receptor's stability, or melting temperature (T_m), remains the single most predictive metric for identifying promising candidate ligands for crystallization trials, with 92% of crystallized ligand-receptor pairs possessing a T_m above 55°C (Alexandrov et al., 2008; Zhang et al., 2015). Yet the mechanism by which select ligands stabilize the receptor and facilitate GPCR crystallogenesis is not well understood.

To examine the relationship between ligand-induced GPCR stabilization and crystallogenesis, a receptor with an array of structurally diverse, high-affinity ligands such as the nociceptin/orphanin FQ (N/OFQ) peptide receptor (NOP) is ideal. NOP is a member of the opioid receptor subfamily of GPCRs that has emerged as a key drug target due to its developing role in pain transmission, drug addiction, anxiety, as well as locomotor and mood disorders (Lambert, 2008). Small-molecule antagonists targeting NOP are under intense investigation for their use as antidepressants (Gavioli and Calo, 2013), while NOP agonists have shown promise as powerful analgesics that lack abuse liability (Lin and Ko,

2013). The crystal structure of human NOP in complex with the potent antagonist Banyu Compound-24 (C-24) was recently solved to a resolution of 3.0 Å, revealing the first atomic details of the receptor as well as specific contacts made by C-24 within the orthosteric binding site (Thompson et al., 2012).

Correlating T_m with a ligand's biochemical and functional properties may help to explain the mechanism behind successful crystallogenesis and expedite selection of the most favorable ligands for structural studies.

Results and Discussion

Distribution of Ligand Properties

Since its discovery in 1994, drug-discovery efforts targeting NOP have produced a variety of agonists and antagonists in the form of both small molecules and peptides (Mollereau et al., 1994; Mustazza and Bastanzio, 2011). Fortuitously, many of these structurally diverse ligands have high affinities, with dozens of ligands possessing K_i values in the low to sub-nM range.

Using the established CPM thermal stability assay (Alexandrov et al., 2008), we measured the melting temperatures of 19 NOP-ligand pairs and evaluated these results with respect to the ligand's MW, calculated LogD, and pK_i. As shown in Figure 1A, we observed no correlation between molecular weight and ligand-induced thermal stability of NOP. Likewise, lipophilicity, given as the pH- and pKa-dependent calculated octanol-water partition coefficient LogD, also did not correlate with receptor stability (Figure 1B). Finally, although single digit nanomolar affinities were necessary for high thermal stabilities, high binding affinities alone were not sufficient for inducing receptor stabilization, with some high-affinity ligands such as UFP-101 ($pK_i > 10$) conferring limited receptor stability (Figure 1C) (Malfacini, 2015; McDonald et al., 2003). These results suggest that although many NOP ligands were developed with exceptional drug-like characteristics, their use in structural studies may be limited by their poor T_m values.

Focusing on the six highest affinity NOP antagonists, we used bioluminescent resonance energy transfer (BRET) to measure the ability of NOP antagonists to inhibit agonist-induced receptor/G protein interactions (Figure 1D, Figure S2). Rankings of BRET-derived antagonist potencies agreed with those obtained from different functional assays investigating recombinant human (calcium mobilization studies in cells expressing chimeric G proteins) as well as native animal (in electrically stimulated mouse vas deferens) NOP receptors (Fischetti et al., 2009; Goto et al., 2006; McDonald et al., 2002; Spagnolo et al., 2007; Trapella et al., 2009; Trapella et al., 2006). Comparing these values to NOP-ligand complex thermal stability results, we observed that antagonist potency (pK_B) and receptor thermal stability (Tm) are positively correlated (linear regression $r^2 = 0.97$, $P < 0.001$).

NOP in Complex with Antagonists SB-612111 and C-35

Having identified SB-612111 and Compound-35 (C-35) as the two next most promising ligands for crystallogenesis, we used lipidic cubic phase (LCP) crystallization to determine

the structure of NOP in complex with these two antagonists, both to a resolution of 3.0 Å (crystallographic statistics in Table 1).

The piperidine-based antagonist SB-612111 is a popular tool compound in *in vitro* and *in vivo* studies of NOP due to its high affinity (pK_i = 9.18) and selectivity (>1000-fold) towards NOP over classical opioid receptors (Spagnolo et al., 2007). The diverse therapeutic potential of SB-612111 has been demonstrated through multiple animal studies in which it has been shown to act as an antidepressant (Rizzi et al., 2007), reduce morphine tolerance (Zaratin et al., 2004), promote antiparkinsonian effects (Marti et al., 2013), and ameliorate colitis in animal models of inflammatory bowel diseases (Alt et al., 2012). Compound C-35 bridges the chemical space between SB-612111 and the previously co-crystallized antagonist C-24, combining the dichlorophenyl head group of SB-612111 with the N-benzyl D-Pro tail from C-24 (chemical structures in Table S2). During *in vitro* assays, C-35 displayed high affinity (pK_i = 9.14) and selectivity (>300-fold) towards NOP over classical opioid receptors (Fischetti et al., 2009).

A summary of specific ligand-receptor interactions is presented in Figure 2. In both the SB-612111 and C-35-bound structures, NOP adopts a very similar conformation as in the previously determined NOP–C24 structure with overall root-mean square deviations (RMSDs) of 0.37 Å (NOP–SB/NOP–C24), and 0.45 Å (NOP–C35/NOP–C24) over receptor Cα atoms (Figure 2A).

Antagonist SB-612111 (Figure 2B) is bound by a salt bridge between the protonated nitrogen of the piperidine and $D130^{3.32}$ (superscripts following residues indicate Ballesteros-Weinstein numbering throughout the text (Ballesteros and Weinstein, 1995) in a mode that resembles that of C-24 (Thompson et al., 2012). The dichlorophenyl head group of SB-612111 is buried deep within the hydrophobic sub-pocket outlined by residues $M134^{3.36}$, $F135^{3.37}$, $I219^{5.42}$, and $V283^{6.55}$, while it's relatively short heterocyclic tail lies flat against $Q107^{2.60}$ at the base of the pocket but does not make direct polar interactions with the receptor. A region of strong electron density in the pocket within the transmembrane core of NOP–SB-612111 is flanked by residues $D97^{2.50}$, $N133^{3.35}$, $S137^{3.39}$, and $N311^{7.45}$ (Figure S3). This density is consistent with that of the sodium ion and water cluster identified in the closely related δ-opioid receptor and several other class A GPCRs (Katritch et al., 2014), though a higher resolution structure is required to unambiguously resolve sodium coordination in NOP.

The binding pose of C-35 (Figure 2C) is similar overall to that of SB-612111, with its piperidine nitrogen forming a salt bridge interaction with $D130^{3.32}$ and a hydrogen bond between its amide nitrogen and $Q107^{2.60}$. The dichlorophenyl head group of C-35 is shifted slightly (~0.8 Å) from that of SB-612111 within the hydrophobic sub-pocket.

All three co-crystallized ligands (SB-612111, C-35, and C-24) contain a piperidine group whose protonated nitrogen participates in a salt bridge interaction with $D130^{3.32}$. Piperidine is a ubiquitous building block in NOP ligand design (Mustazza and Bastanzio, 2011), and the piperidine-$D130^{3.32}$ salt bridge common to these structures offers a direct rationalization for the high affinities of this ligand class.

Although the D130$^{3.32}$ residue is conserved in all four opioid receptors, it plays a crucial role in binding of the highly selective endogenous agonist N/OFQ (Mouledous et al., 2000; Thompson et al., 2012). Because of this, interactions between D130$^{3.32}$ and ligands likely contribute to affinity rather than efficacy or selectivity. Notably, the head group of the antagonists described here (a spiroisobenzofuran in C-24 and a dichlorophenyl in C-35 and SB-612111) lies perpendicular to this piperidine ring in all cases – a structural feature previously suggested to be of importance to NOP ligand affinity and efficacy (Trapella et al., 2009).

Docking Studies: Degenerate Ligand Binding Modes Correlate with Low Receptor Stability

In order to better understand the nature of stabilizing receptor interactions with antagonists and potential conformational changes in the receptor upon their binding, we performed molecular docking of several additional antagonists. We first validated our docking protocol by cross-docking the co-crystallized antagonist in Figure 2 against all three NOP structures in the context of both rigid and flexible receptor side chains. Cross-docking of antagonists C-35, SB-612111, and C-24 into all crystal structures of NOP resulted in accurately reproduced binding poses with RMSDs ranging from 0.6 to 1.3 Å (Table S3). Moreover, energy–based refinement of these compounds with extensive flexible sampling of binding pocket side chains resulted in only very minor variations in receptor and ligand conformations.

In contrast, docking of antagonist J-113397 and key derivatives based on the compound's 4-(2-keto-1-benzimidazolinyl)-piperidine scaffold suggests substantial differences in the receptor interactions with compounds of this chemotype (Kawamoto et al., 1999). Docking of J-113397 into the rigid NOP structure led to an unexpected, flipped orientation (deemed mode II) of the piperidine ring as compared to co-crystallized ligands (Figure 3A, **right panel**). Analysis of this binding mode suggests that the ethyl moiety on J-113397's benzimidazolinyl ring prevents it from binding in the unflipped orientation (mode I) due to a severe steric clash between the ethyl group and the Q280$^{6.52}$ side chain. However, allowing conformational sampling of receptor side chains and water during docking allowed J-113397 to bind in an orientation similar to the co-crystallized ligands (mode I), with a comparable free energy of binding (Figure 3A, left panel).

Similar to J-113397, a flip between predicted rigid and flexible receptor docking conformations was observed for Trap-101 (Figure 3B), an achiral analogue of J-113397 with a double bond introduced between C3 and C4 positions of the piperidine ring (Trapella et al., 2006). Interestingly, the 3-hydroxymethyl moiety of J-113397 and Trap-101 in mode I points deep into the pocket, forming additional hydrogen bonds with both the D130$^{3.32}$ side chain and the adjacent water molecule observed in the crystal structure (Figure S4). This tight binding of the 3-hydroxymethyl group is supported by previous SAR studies, which show that replacement of the 3-hydroxymethyl with a bulkier $COOCH_3$ moiety reduces binding of both J-113397 and Trap-101 by about 100 fold (Trapella et al., 2006). The residual binding of the Trap-101 3-$COOCH_3$ derivative suggest that this chemotype can still bind in an alternative conformation, likely similar to the flipped, mode II conformation observed in rigid docking, albeit with greatly reduced affinity. Multiple predicted binding

modes were also observed for high affinity antagonist JTC-801, which adopted a distinct binding mode buried in the crevice between helices 4 and 5 (Figure S4).

A Mechanism for Stabilization: Ligand-Receptor Conformational Pairs

Analysis of the above docking results (Figure 3) in the context of thermostability data for these ligands (Figure 1) suggests that the tight and unique binding poses of compounds like C-24, C-35 and SB-612111 may be one of the prerequisites for complex thermostabilization and conformational stabilization that are critical for successful crystallogenesis. Thus, compounds with at least two predicted alternative binding poses J-113397, Trap-101, and JTC-801, had reduced T_m values and were not amenable for crystallization.

Interestingly, the peptide antagonist UFP-101 was not shown to significantly stabilize NOP despite its exceptional sub-nanomolar affinity (Figure 1D) (McDonald et al., 2003). Docking of UFP-101 in our previous study (Thompson et al., 2012) showed that its interactions with NOP were primarily electrostatic in nature, with multiple positively charged residues in the C terminus (residues 5–17) of UFP-101 binding to negatively charged receptor side chains at the entrance of the binding pocket. Such interactions are likely to be non-specific, with the numerous rotatable bonds of UFP-101 allowing alternative salt-bridge pairings of positively and negatively charged side chains, which further corroborates the potential link between the multiplicity of ligand binding conformations and reduced thermostability.

Future Outlook: Ligand-Receptor Interactions and Crystallization

Understanding GPCR signal transduction begins with detailed knowledge of ligand-receptor interactions. Toward this aim, identification of ligands that facilitate crystallogenesis for GPCR structural studies is a major bottleneck, and has been limited by our lack of understanding surrounding receptor stabilization and its connection to crystallogenesis.

High receptor thermal stability (T_m) has become a hallmark of pre-crystallization trials for GPCRs, as ligands that stabilize the receptors are thought to aid in folding and increase dwell time of the receptor in the desired conformational state. The linear relationship between ligand-induced thermal stability (T_m) and antagonist potency (pK_B) provides us with another potential avenue by which candidate ligands for crystallization may be identified. Unlike T_m measurements, pK_B values derived from BRET assays can be measured using crude membrane preparations, and in the case of β-arrestin variations on the assay, whole cells, such that protein purification is no longer required. Due to the ease of sample preparation, the BRET assay is more amenable to adaptation as a high-throughput tool for ligand screening purposes specifically for GPCR structural studies.

Intensifying efforts to determine the relationship between conformational heterogeneity and receptor stability have resulted in a wealth of hypotheses surrounding the mechanism of GPCR activation, as well as the influence of ligands on these processes (Bock et al., 2014; Liu et al., 2012; Manglik et al., 2015; Nygaard et al., 2013; Vaidehi et al., 2014). In the present study, we determined the crystal structures of NOP in complex with antagonists SB-612111 and C-35, extending the findings of the previously reported antagonist-bound structure of NOP bound to C-24. We also demonstrate a strong correlation between antagonist pK_B and thermostability, thus highlighting a high throughput strategy for

identifying GPCR ligands for crystallization. The increase in thermostability is consistent with a reduction in receptor flexibility by shifting the conformational equilibrium exclusively to the antagonized state. Docking studies indicate that these potent antagonists, such as SB-612111, have a single permissible binding mode which promotes a uniform local conformation, high receptor stability, and isolation via crystallization (Figure 4A). In contrast, ligands that adopt multiple binding poses (such as J-113397, Trap-101, JTC-801, and UFP-101) divide the receptor population by the number of binding orientations (Figure 4B); the resulting conformational heterogeneity decreases receptor stability as well as the probability of isolating one receptor-ligand conformational pair via crystallization.

Because GPCRs maintain a dynamic equilibrium between several conformational states corresponding to various signaling events (Audet and Bouvier, 2012; Liu et al., 2012), an analogous link between the degeneracy of receptor-ligand conformational pairs and crystallization could potentially be extended to active-state receptors. While the multiplicity of ligand binding modes stunts crystallization of inactive-state (antagonist-bound) receptors, this degeneracy is further amplified in the presence of agonists by virtue of multiple active-state conformations (Manglik et al., 2015). Thus, selecting an agonist with a single preferred binding orientation and strong functional selectivity towards one signaling pathway over others may boost receptor conformational homogeneity and the likelihood of crystallogenesis.

Together our results not only suggest a potential mechanism for antagonist-induced receptor stabilization, but also point to new avenues for identifying receptor-ligand pairs that are most amenable to structural studies. Such advances in our understanding of ligand-receptor interactions will aid in the goal of understanding GPCR structural biology.

Experimental Procedures

Chemical Compounds

The N/OFQ peptide was synthesized in house following the procedures previously described in detail (Guerrini et al., 1997). The non-peptide molecules C-35, C-24, Trap-101 and J-113397 were synthesized in house by C. Trapella. SB-612111 was from Tocris bioscience (Bristol, UK). All tissues culture media and supplements were from Invitrogen (Paisley, UK). Reagents used were from Sigma Chemical Co. (Poole, UK) or E. Merck (Darmstadt, Germany) and were of the highest purity available. Native coelenterazine (CLZN, 5 mM, EtOH) was from Synchem UG & Co. KG (Altenburg, Germany). N/OFQ was dissolved in ultrapure water (1 mM) while other ligands were dissolved in dimethyl sulfoxide (10 mM) and kept at −20 °C until use.

Cell and Membrane Preparation for BRET Assay

Human Embryonic Kidney (HEK293) cells were grown in Dulbecco's modified Eagle's medium, supplemented with 10% (v/v) fetal calf serum, 100 units/ml penicillin G, and 100 ng/ml streptomycin sulfate, in a humidified atmosphere of 5% CO_2 at 37 °C. Cell lines permanently co-expressing NOP-RLuc and $G\beta_1$-RGFP were prepared using the pantropic

retroviral expression system by Clontech as described previously (Malfacini, 2015; Molinari et al., 2008).

NOP/G protein interaction experiments were performed in enriched plasma membrane aliquots from transfected cells prepared by differential centrifugation. In brief, cells were detached with PBS/EDTA solution (1 mM, pH 7.4 NaOH) then, after 5 min of 500 g centrifugation, Dounce-homogenized (30 strokes) in cold homogenization buffer (TRIS 5 mM, EGTA 1 mM, DTT 1 mM, pH 7.4 adjusted with HCl) in the presence of sucrose (0.32 M). Three following centrifugations were performed at 1000 g (4 °C) and supernatants kept. Two 25,000 g (4 °C) subsequent centrifugations (the second in the absence of sucrose) were performed for separating enriched membranes that, after discarding the supernatant, were kept in ultrapure water at −80 °C (Vachon et al., 1987). The protein concentration in membranes was determined using the QPRO - BCA kit (Cyanagen Srl, Bologna, IT) and Beckman DU 520 spectrophotometer (Brea, CA, USA).

Bioluminescent Resonance Energy Transfer (BRET) Assays

Membrane bioluminescence was recorded in 96-well untreated white opaque microplates (PerkinElmer, Waltham, MA, USA). For the determination of NOP/G protein interaction, membranes (3 μg of protein) prepared as described above were added to wells in Dulbecco's PBS (DPBS). NOP/G protein interactions were measured in the presence of CLZN (5 μM, injected 10 min prior reading the cell plate) in cell membranes; the contribution of other cellular processes (i.e. arrestin recruitment, internalization) was hence negligible. Increasing concentrations of N/OFQ were added in 20 μL of PBS - BSA 0.01 % (Bovine Serum Albumin, Sigma Chemical Co. (Poole, UK)) 15 min before reading luminescence. Luminescence signals were measured as counts per second (CPS) with a Victor X 2030 luminometer (PerkinElmer, Waltham, MA, USA). Emissions were selected using 460 nm (25 nm bandwidth) and 510 nm (10 nm bandwidth) bandpass filters for Rluc and RGFP, respectively. All BRET experiments were performed at room temperature.

BRET Assay Data Analysis

Concentration-response curves to N/OFQ were carried out in absence and in presence of a fixed concentration of each antagonist. Antagonists were added to membranes 15 min prior the addition of concentration-response curves to N/OFQ. Following agonist injection, re-equilibration was allowed by leaving agonist/antagonist competing for 15 min before the measurement of BRET ratio. All data were computed as stimulated BRET ratio units, i.e. the ratio between counts per second (CPS) from RGFP and RLuc in the presence of ligands, followed by baseline subtraction, i.e. the BRET value in the absence of ligand.

Maximal agonist effects (E_{max}) were expressed as fraction of the N/OFQ E_{max} which was determined in every assay plate and reported as E/E_{max}, in the graphs available in the Supplemental Experimental Procedures. Concentration-response curves to agonists and inhibition response curves to antagonists were analyzed with a four-parameter logistic nonlinear regression model. Agonist data are expressed as mean ± SEM of *n* experiments.

Antagonist potencies were derived with the following equation: $pK_B = (\log(CR - 1)) - \log[[B]]$ where CR is the ratio between agonist potency (expressed as EC_{50}) in the presence and absence of antagonist and [B] is the molar concentration of antagonist. Antagonist pK_B values were derived from at least 4 experiments performed in duplicate are reported as mean ± $CL_{95\%}$. The value pK_B is the negative logarithm of the equilibrium dissociation constant of an antagonist-receptor complex as determined through a functional assay in which a physiological response is antagonized. In other words, K_B is the concentration of antagonist that occupies half of the receptor population at equilibrium, expressed in units *M*. Curve fitting was performed using PRISM 5.0 (GraphPad Software Inc., San Diego, USA).

Protein Expression and Purification for Crystallogenesis

The human NOP receptor structures presented here use a previously described fusion-partner construct and expression scheme (Thompson et al., 2012). Details of receptor expression and purification are available in the Supplemental Experimental Procedures. Receptor purity and monodispersity were monitored via SDS–PAGE and analytic size exclusion chromatography throughout purification. Typically, protein from 5 L of *Spodoptera frugiperda* (*Sf*9) insect cell biomass was concentrated to 20 μL in order to yield a concentrated solution of 40 mg/ml appropriate for one round of crystallization.

Lipidic Cubic Phase Crystallization

Concentrated protein samples were reconstituted into lipidic cubic phase (LCP) by mixing with molten lipid using a mechanical syringe mixer at room temperature (~20–22 °C) (Caffrey and Cherezov, 2009). The LCP mixture contained 40% (w/w) concentrated protein, 54% (w/w) monoolein (Sigma), and 6% (w/w) cholesterol (AvantiPolar Lipids). Crystallization trials were performed in 96-well glass sandwich plates (Marienfeld) (Cherezov et al., 2004) onto which 40 nl protein-containing LCP drops and 0.8 μl precipitant solution were deposited by the NT8-LCP (Formulatrix) or mosquito LCP (TTP Labtech) crystallization robots. The crystallization plates were then sealed with a glass cover slip and stored at 20 °C in an incubator/imager (RockImager 1000, Formulatrix). Diffraction quality crystals were grown and harvested after about ~20 days in 25–35% (v/v) PEG400, 130–200 mM potassium sodium tartrate tetrahydrate, 100 mM Bis-Tris propane, pH 6.4. Crystals were collected directly from LCP using 50 μm MiTeGen micromounts and immediately flash frozen in liquid nitrogen.

X-ray Data Collection and Processing

X-ray data were collected at the 23ID-B/D beamline (GM/CA CAT) at the Advanced Photon Source, Argonne National Laboratory, using a 10 μm collimated minibeam with X-ray wavelength of 1.0330 Å and a MarMosaic 300 CCD detector. Due to radiation damage, typically 10–20° wedges of data were collected from each crystal at 100 K using an unattenuated beam, with 1° of oscillation and 1–2 sec exposure, before changing the crystal.

Structure Determination and Refinement

Initial phases were obtained by molecular replacement with Phaser-MR (McCoy, 2007) maximum likelihood molecular replacement using the original NOP–C24 structure as a

search model (PDB ID: 4EA3, ligands removed, BRIL and transmembrane domains searched for separately). Each asymmetric unit contains two antiparallel receptors and one BRIL fusion partner. The second BRIL fusion was not observed in any of the reported NOP structures, likely due to disorder. Model building was performed with Coot (Emsley et al., 2010), while structural refinement was carried out with PHENIX (Adams et al., 2010). Crystallographic R_{work}, as well as R_{free} for 5% of the reflections excluded from the refinement, were calculated to monitor the structural refinement procedures. The results of the structural analysis are summarized in Table 1. Structural validation was performed using Molprobity (Chen et al., 2010). All molecular graphics were produced with PyMOL molecular graphics system v.1.4.1 (Schroedinger).

Docking Assessment of Crystal Structures

Both rigid and flexible docking of small molecule ligands into the available crystal structures of NOP were performed using Internal Coordinate Mechanics (ICM) molecular modeling suite (Tables S2, S3, Figure S4) (Abagyan et al., 1994; Abagyan et al., 2009). For the rigid receptor docking, receptor models were prepared from crystal structures by assigning and optimizing conformations of hydrogen atoms and generating the set of grid potential maps of the receptor in a 30×30×30 Å box covering the extracellular half of the receptor. Ligand docking is based on biased probability Monte Carlo (BPMC) optimization of the ligand internal coordinates (Totrov and Abagyan, 1997). Compounds in two-dimensional representation were converted to 3D and energy optimized using MMFF-94 force field (Halgren, 1995); at least ten random orientations of the ligand were used as starting conformations. Monte Carlo sampling and optimization was performed at high thoroughness=30. The objective energy function included the ligand internal strain and a weighted sum of the grid map values in ligand atom centers. For the flexible receptor docking, we used an explicit all-atom representation of the receptor, where side chains within 6 Å of the ligand were considered flexible. Extensive sampling of the ligand and side chain conformations in the binding pocket was performed using ICM global energy optimization (Totrov and Abagyan, 1997).

To ensure convergence of the Monte Carlo optimization, five independent runs of the docking procedure were performed, and the resulting poses compared. The docking results individual docking runs for each compound were considered consistent if at least three of the docking runs produced similar ligand conformations with RMSD < 2.0 Å and Binding Score < −14.0 kJ/mol. The ICM ligand Binding Score (Bursulaya et al., 2003; Schapira et al., 1999) was calculated as:

$$S_{bind}=E_{int}+T\Delta S_{Tor}+E_{vw}+\alpha_1 \times E_{el}+\alpha_2 \times E_{hb}+\alpha_3 \times E_{hb}+\alpha_4 \times E_{sf}$$

where E_{vw}, E_{el}, E_{hb}, E_{hp}, and E_{sf} are Van der Waals, electrostatic, hydrogen bonding, non-polar and polar atom solvation energy differences between bound and unbound states, E_{int} is the ligand internal strain, ΔS_{Tor} is its conformational entropy loss upon binding, T = 300 K, and α_i are ligand- and receptor-independent constants. No distance restraints or any other experimentally derived information was used in the ligand docking procedure.

Supplementary Material

Refer to Web version on PubMed Central for supplementary material.

Acknowledgments

The authors gratefully acknowledge Gustavo Fenalti, Wei Liu, Enrique Abola, Angela Walker, and Lukas Sušac for helpful discussion. We also thank Tam Trinh and Meihua Chu for support with protein expression, as well as Tommaso Costa for the preparation of the cell clones used for pharmacological studies. The GM/CA-CAT beamline (23-ID/B) is supported by the National Cancer Institute (Y1-CO-1020) and the National Institute of General Medical Sciences (Y1-GM-1104). This research was supported in part by NIH Common Fund grant P50 GM073197, Protein Structure Initiative grant U54 GM094618 for structure production, as well as the Italian Ministry of University and Scientific Research FIRB grant RBFR109SBM.

References

Abagyan R, Totrov M, Kuznetsov D. Icm - a New Method for Protein Modeling and Design - Applications to Docking and Structure Prediction from the Distorted Native Conformation. J Comput Chem. 1994; 15:488–506.

Abagyan, RA.; Orry, A.; Raush, E.; Budagyan, L.; Totrov, M. ICM Manual. La Jolla, CA: MolSoft LLC; 2009.

Adams PD, Afonine PV, Bunkoczi G, Chen VB, Davis IW, Echols N, Headd JJ, Hung LW, Kapral GJ, Grosse-Kunstleve RW, et al. PHENIX: a comprehensive Python-based system for macromolecular structure solution. Acta Crystallogr D Biol Crystallogr. 2010; 66:213–221. [PubMed: 20124702]

Alexandrov AI, Mileni M, Chien EY, Hanson MA, Stevens RC. Microscale fluorescent thermal stability assay for membrane proteins. Structure. 2008; 16:351–359. [PubMed: 18334210]

Alt C, Lam JS, Harrison MT, Kershaw KM, Samuelsson S, Toll L, D'Andrea A. Nociceptin/orphanin FQ inhibition with SB612111 ameliorates dextran sodium sulfate-induced colitis. Eur J Pharmacol. 2012; 683:285–293. [PubMed: 22449384]

Audet M, Bouvier M. Restructuring G-protein- coupled receptor activation. Cell. 2012; 151:14–23. [PubMed: 23021212]

Ballesteros J, Weinstein H. Integrated methods for the construction of three-dimensional models and computational probing of structure-function relations in G protein-coupled receptors. Methods Neurosci. 1995; 25:366–428.

Bock A, Chirinda B, Krebs F, Messerer R, Batz J, Muth M, Dallanoce C, Klingenthal D, Trankle C, Hoffmann C, et al. Dynamic ligand binding dictates partial agonism at a G protein-coupled receptor. Nat Chem Biol. 2014; 10:18–20. [PubMed: 24212135]

Bursulaya BD, Totrov M, Abagyan R, Brooks CL 3rd. Comparative study of several algorithms for flexible ligand docking. J Comput Aided Mol Des. 2003; 17:755–763. [PubMed: 15072435]

Caffrey M, Cherezov V. Crystallizing membrane proteins using lipidic mesophases. Nat Protoc. 2009; 4:706–731. [PubMed: 19390528]

Chen VB, Arendall WB 3rd, Headd JJ, Keedy DA, Immormino RM, Kapral GJ, Murray LW, Richardson JS, Richardson DC. MolProbity: all-atom structure validation for macromolecular crystallography. Acta Crystallogr D Biol Crystallogr. 2010; 66:12–21. [PubMed: 20057044]

Cherezov V, Peddi A, Muthusubramaniam L, Zheng YF, Caffrey M. A robotic system for crystallizing membrane and soluble proteins in lipidic mesophases. Acta Crystallogr D Biol Crystallogr. 2004; 60:1795–1807. [PubMed: 15388926]

Emsley P, Lohkamp B, Scott WG, Cowtan K. Features and development of Coot. Acta Crystallogr D Biol Crystallogr. 2010; 66:486–501. [PubMed: 20383002]

Fischetti C, Camarda V, Rizzi A, Pela M, Trapella C, Guerrini R, McDonald J, Lambert DG, Salvadori S, Regoli D, et al. Pharmacological characterization of the nociceptin/orphanin FQ receptor non peptide antagonist Compound 24. Eur J Pharmacol. 2009; 614:50–57. [PubMed: 19445927]

Gavioli EC, Calo G. Nociceptin/orphanin FQ receptor antagonists as innovative antidepressant drugs. Pharmacol Ther. 2013; 140:10–25. [PubMed: 23711793]

Goto Y, Arai-Otsuki S, Tachibana Y, Ichikawa D, Ozaki S, Takahashi H, Iwasawa Y, Okamoto O, Okuda S, Ohta H, et al. Identification of a novel spiropiperidine opioid receptor-like 1 antagonist class by a focused library approach featuring 3D-pharmacophore similarity. J Med Chem. 2006; 49:847–849. [PubMed: 16451050]

Guerrini R, Calo G, Rizzi A, Bianchi C, Lazarus LH, Salvadori S, Temussi PA, Regoli D. Address and message sequences for the nociceptin receptor: a structure-activity study of nociceptin-(1-13)-peptide amide. J Med Chem. 1997; 40:1789–1793. [PubMed: 9191955]

Halgren T. Merck molecular force field I-V. J Comp Chem. 1995; 17:490–641.

Katritch V, Fenalti G, Abola EE, Roth BL, Cherezov V, Stevens RC. Allosteric sodium in class A GPCR signaling. Trends Biochem Sci. 2014; 39:233–244. [PubMed: 24767681]

Kawamoto H, Ozaki S, Itoh Y, Miyaji M, Arai S, Nakashima H, Kato T, Ohta H, Iwasawa Y. Discovery of the first potent and selective small molecule opioid receptor-like (ORL1) antagonist: 1-[(3R,4R)-1-cyclooctylmethyl-3- hydroxymethyl-4-piperidyl]-3-ethyl-1, 3-dihydro-2H-benzimidazol-2-one (J-113397). J Med Chem. 1999; 42:5061–5063. [PubMed: 10602690]

Lambert DG. The nociceptin/orphanin FQ receptor: a target with broad therapeutic potential. Nat Rev Drug Discov. 2008; 7:694–710. [PubMed: 18670432]

Lin AP, Ko MC. The therapeutic potential of nociceptin/orphanin FQ receptor agonists as analgesics without abuse liability. ACS Chem Neurosci. 2013; 4:214–224. [PubMed: 23421672]

Lipinski CA. Lead- and drug-like compounds: the rule-of-five revolution. Drug Discov Today Technol. 2004; 1:337–341. [PubMed: 24981612]

Liu JJ, Horst R, Katritch V, Stevens RC, Wuthrich K. Biased signaling pathways in beta2-adrenergic receptor characterized by 19F-NMR. Science. 2012; 335:1106–1110. [PubMed: 22267580]

Malfacini D, Ambrosio C, Gro MC, Sbraccia M, Trapella C, Guerrini R, Broide R, Francis J, Bonora M, Pinton P, Costa T, Calo G. Pharmacological Profile of Nociceptin/Orphanin FQ Receptors Interacting with G-Proteins and β-Arrestins 2. PLoS One. 2015; 10:e0132865. [PubMed: 26248189]

Manglik A, Kim TH, Masureel M, Altenbach C, Yang Z, Hilger D, Lerch MT, Kobilka TS, Thian FS, Hubbell WL, et al. Structural Insights into the Dynamic Process of beta2-Adrenergic Receptor Signaling. Cell. 2015; 161:1101–1111. [PubMed: 25981665]

Marti M, Mela F, Budri M, Volta M, Malfacini D, Molinari S, Zaveri NT, Ronzoni S, Petrillo P, Calo G, et al. Acute and chronic antiparkinsonian effects of the novel nociceptin/orphanin FQ receptor antagonist NiK-21273 in comparison with SB-612111. Br J Pharmacol. 2013; 168:863–879. [PubMed: 22994368]

McCoy AJ. Solving structures of protein complexes by molecular replacement with Phaser. Acta Crystallogr D Biol Crystallogr. 2007; 63:32–41. [PubMed: 17164524]

McDonald J, Barnes TA, Calo G, Guerrini R, Rowbotham DJ, Lambert DG. Effects of [(pF)Phe(4)]nociceptin/orphanin FQ-(1-13)NH(2) on GTPgamma(35)S binding and cAMP formation in Chinese hamster ovary cells expressing the human nociceptin/orphanin FQ receptor. Eur J Pharmacol. 2002; 443:7–12. [PubMed: 12044785]

McDonald J, Calo G, Guerrini R, Lambert DG. UFP-101, a high affinity antagonist for the nociceptin/orphanin FQ receptor: radioligand and GTPgamma(35)S binding studies. Naunyn Schmiedebergs Arch Pharmacol. 2003; 367:183–187. [PubMed: 12595960]

Molinari P, Casella I, Costa T. Functional complementation of high-efficiency resonance energy transfer: a new tool for the study of protein binding interactions in living cells. Biochem J. 2008; 409:251–261. [PubMed: 17868039]

Mollereau C, Parmentier M, Mailleux P, Butour JL, Moisand C, Chalon P, Caput D, Vassart G, Meunier JC. ORL1, a novel member of the opioid receptor family. Cloning, functional expression and localization. FEBS Lett. 1994; 341:33–38. [PubMed: 8137918]

Mouledous L, Topham CM, Mazarguil H, Meunier JC. Direct identification of a peptide binding region in the opioid receptor-like 1 receptor by photoaffinity labeling with [Bpa(10),Tyr(14)]nociceptin. J Biol Chem. 2000; 275:29268–29274. [PubMed: 10880520]

Mustazza C, Bastanzio G. Development of nociceptin receptor (NOP) agonists and antagonists. Med Res Rev. 2011; 31:605–648. [PubMed: 20099319]

Nygaard R, Zou Y, Dror RO, Mildorf TJ, Arlow DH, Manglik A, Pan AC, Liu CW, Fung JJ, Bokoch MP, et al. The dynamic process of beta(2)-adrenergic receptor activation. Cell. 2013; 152:532–542. [PubMed: 23374348]

Rask-Andersen M, Masuram S, Schioth HB. The druggable genome: Evaluation of drug targets in clinical trials suggests major shifts in molecular class and indication. Annu Rev Pharmacol Toxicol. 2014; 54:9–26. [PubMed: 24016212]

Rizzi A, Gavioli EC, Marzola G, Spagnolo B, Zucchini S, Ciccocioppo R, Trapella C, Regoli D, Calo G. Pharmacological characterization of the nociceptin/orphanin FQ receptor antagonist SB-612111 [(−)-cis-1-methyl-7-[[4-(2,6-dichlorophenyl)piperidin-1-yl]methyl]-6,7,8,9-tetrah ydro-5H-benzocyclohepten-5-ol]: in vivo studies. J Pharmacol Exp Ther. 2007; 321:968–974. [PubMed: 17329551]

Schapira M, Totrov M, Abagyan R. Prediction of the binding energy for small molecules, peptides and proteins. J Mol Recognit. 1999; 12:177–190. [PubMed: 10398408]

Spagnolo B, Carra G, Fantin M, Fischetti C, Hebbes C, McDonald J, Barnes TA, Rizzi A, Trapella C, Fanton G, et al. Pharmacological characterization of the nociceptin/orphanin FQ receptor antagonist SB-612111 [(−)-cis-1-methyl-7-[[4-(2,6-dichlorophenyl)piperidin-1-yl]methyl]-6,7,8,9-tetrah ydro-5H-benzocyclohepten-5-ol]: in vitro studies. J Pharmacol Exp Ther. 2007; 321:961–967. [PubMed: 17329552]

Thompson AA, Liu W, Chun E, Katritch V, Wu H, Vardy E, Huang XP, Trapella C, Guerrini R, Calo G, et al. Structure of the nociceptin/orphanin FQ receptor in complex with a peptide mimetic. Nature. 2012; 485:395–399. [PubMed: 22596163]

Totrov M, Abagyan R. Flexible protein-ligand docking by global energy optimization in internal coordinates. Proteins Suppl. 1997; 1:215–220.

Trapella C, Fischetti C, Pela M, Lazzari I, Guerrini R, Calo G, Rizzi A, Camarda V, Lambert DG, McDonald J, et al. Structure-activity studies on the nociceptin/orphanin FQ receptor antagonist 1-benzyl-N-{3-[spiroisobenzofuran-1(3H),4′-piperidin-1-yl]propyl} pyrrolidine-2-carboxamide. Bioorg Med Chem. 2009; 17:5080–5095. [PubMed: 19527931]

Trapella C, Guerrini R, Piccagli L, Calo G, Carra G, Spagnolo B, Rubini S, Fanton G, Hebbes C, McDonald J, et al. Identification of an achiral analogue of J-113397 as potent nociceptin/orphanin FQ receptor antagonist. Bioorg Med Chem. 2006; 14:692–704. [PubMed: 16202610]

Vachon L, Costa T, Herz A. Opioid receptor desensitization in NG 108-15 cells. Differential effects of a full and a partial agonist on the opioid-dependent GTPase. Biochem Pharmacol. 1987; 36:2889–2897. [PubMed: 2820424]

Vaidehi N, Bhattacharya S, Larsen AB. Structure and dynamics of G-protein coupled receptors. Adv Exp Med Biol. 2014; 796:37–54. [PubMed: 24158800]

Weiss MS. Global indicators of X-ray data quality. J Appl Crystallogr. 2001; 34:130–135.

Zaratin PF, Petrone G, Sbacchi M, Garnier M, Fossati C, Petrillo P, Ronzoni S, Giardina GA, Scheideler MA. Modification of nociception and morphine tolerance by the selective opiate receptor-like orphan receptor antagonist (−)-cis-1-methyl-7-[[4-(2,6-dichlorophenyl)piperidin-1-yl]methyl]-6,7,8,9-tetrahy dro-5H-benzocyclohepten-5-ol (SB-612111). J Pharmacol Exp Ther. 2004; 308:454–461. [PubMed: 14593080]

Zhang X, Stevens RC, Xu F. The importance of ligands for G protein-coupled receptor stability. Trends Biochem Sci. 2015; 40:79–87. [PubMed: 25601764]

Highlights

- A correlation is demonstrated between receptor stability and BRET functional data
- Two antagonist-bound crystal structures of the N/OFQ peptide receptor are reported
- Docking indicates degenerate binding modes contribute to poor receptor stabilization
- A mechanism for antagonist-induced receptor stabilization is proposed

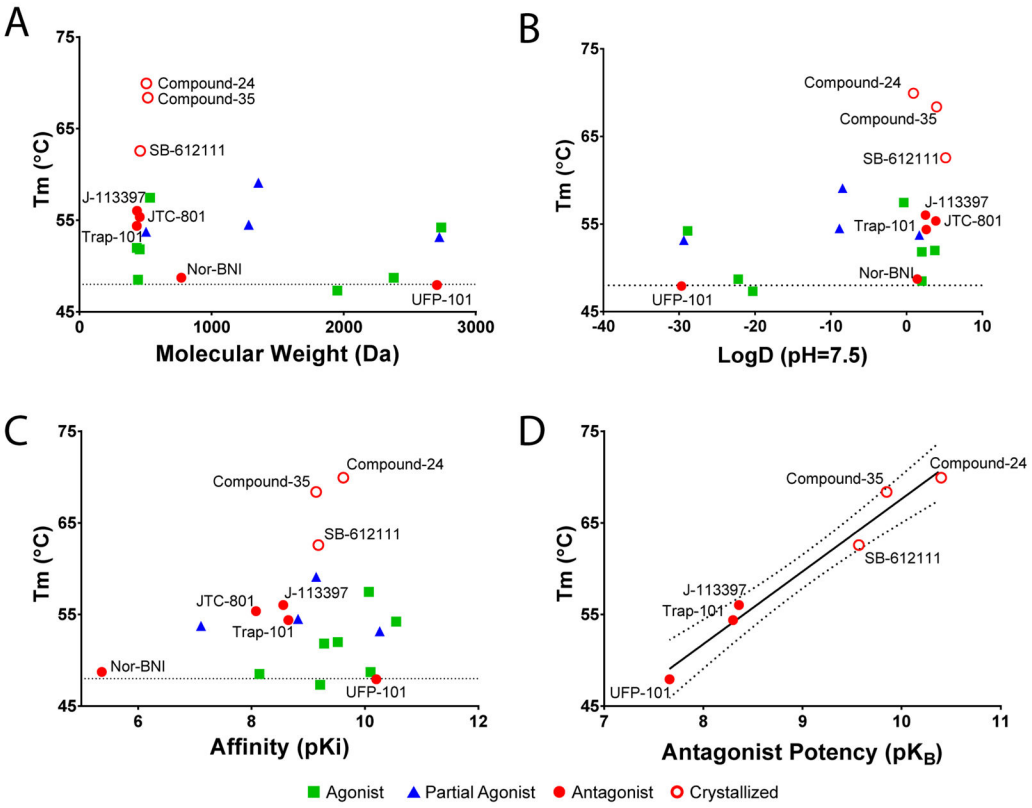

Figure 1. Distribution of NOP ligand metrics in the context of receptor stabilization

Ligand-induced N/OFQ peptide receptor (NOP) stability (melting temperature, T_m in °C) plotted against four ligand properties: (**A**) molecular weight (Da), (**B**) calculated lipophilicity (LogD), (**C**) affinity (pK_i), and (**D**) antagonist potency (pK_B). No correlation is observed between receptor T_m and ligand size or lipophilicity, whereas high (nM-range) ligand affinity is necessary, but not sufficient, to induce receptor stabilization. BRET functional data indicate a positive correlation between antagonist potency and ligand-induced thermal stability (linear regression, $r^2 = 0.9713$ $P < 0.001$ with $CL_{95\%}$ shown). T_m of the ligand-free receptor is indicated as a dotted line at 48 °C. Antagonists are shown as red circles, agonists as green squares, and partial agonists as blue triangles. Empty red circles indicate antagonists for which co-crystal structures could be obtained. Explicit values for all metrics available in Table S1 and primary BRET data are given in Figure S2.

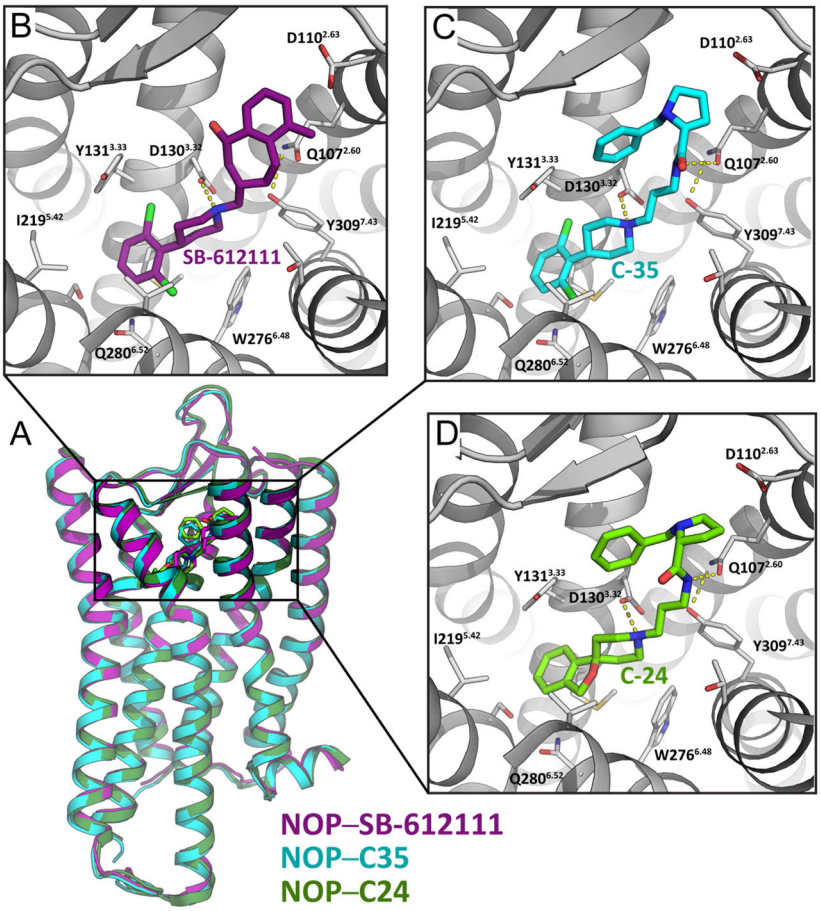

Figure 2. Crystal structures of human NOP bound to thermally stabilizing antagonists

(**A**) NOP co-crystal structure overlay of (**B–D**) ligand binding modes reveals a highly conserved receptor structure when bound to (**B**) SB-612111, purple, (**C**) Compound-35 (C-35), cyan, and (**D**) Banyu Compound-24 (C-24), green. All three piperidine-based antagonists participate in a salt-bridge interaction with $D130^{3.32}$, which anchors them to the base of the orthosteric binding pocket. Ligands and residues around the binding site are represented as sticks with non-carbon atoms colored by atom type (chlorine: green, oxygen: red, nitrogen: blue). Hydrogen bonds are represented as yellow dashed lines. Superscripts indicate the Ballesteros-Weinstein numbering convention (Ballesteros and Weinstein, 1995). See also Figure S3.

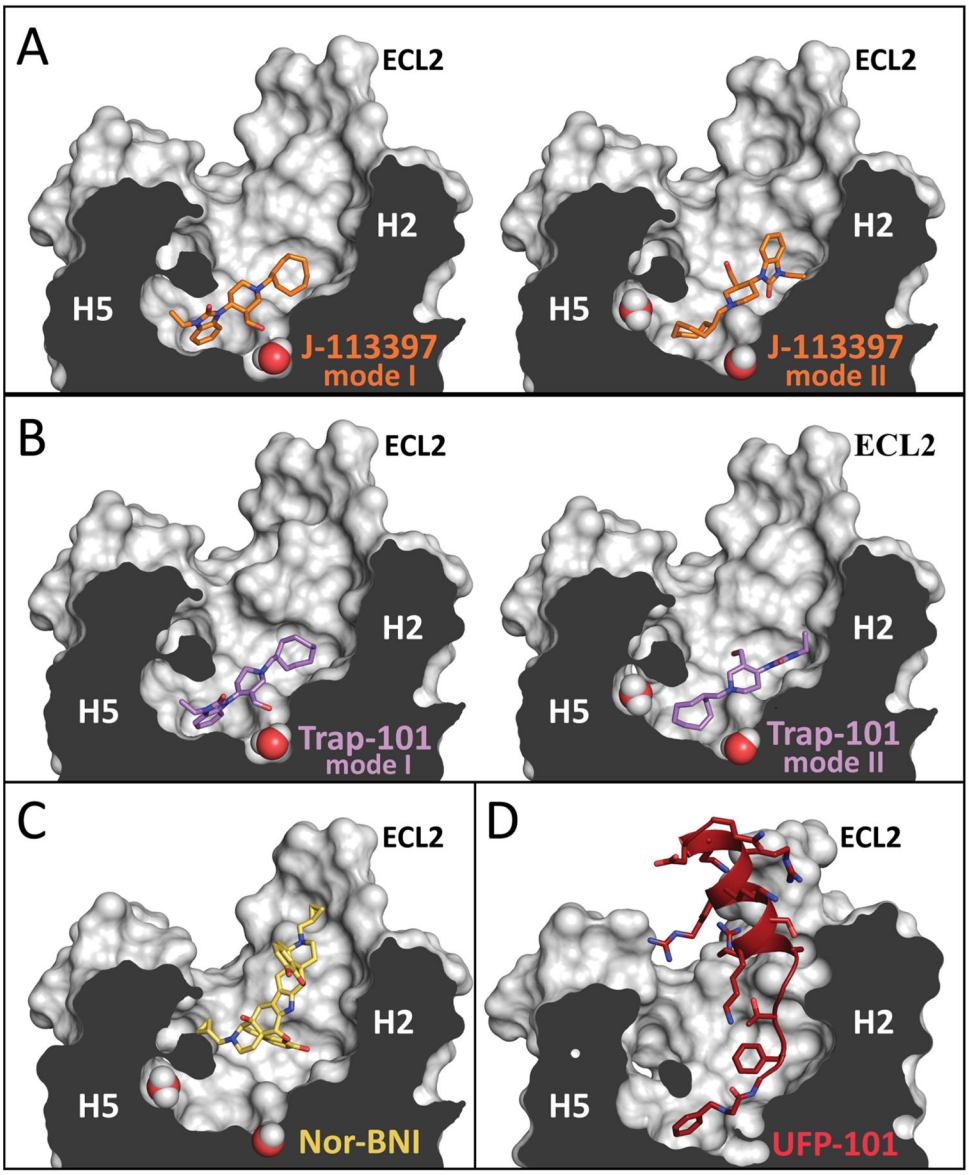

Figure 3. Docking studies reveal multiple binding modes for NOP antagonists and offer clues to their destabilizing nature

Predicted binding modes of compounds (**A**) J-113397, orange, (**B**) Trap-101, violet, (**C**) Nor-BNI, yellow, and (**D**) UFP-101, red, were docked into the NOP model with flexible side chains and water sampling. For J-113397 and Trap-101, two binding modes with comparable free energies were found (mode I: left, “flipped” mode II: right). The locations of transmembrane helices 2 and 5 (H2, H5), along with the extracellular loop 2 (ECL2), are given. Ligand chemical structures are given in Table S2, explicit free energies of binding can be found in Table S3, and detailed ligand-receptor interactions are shown in Figure S4.

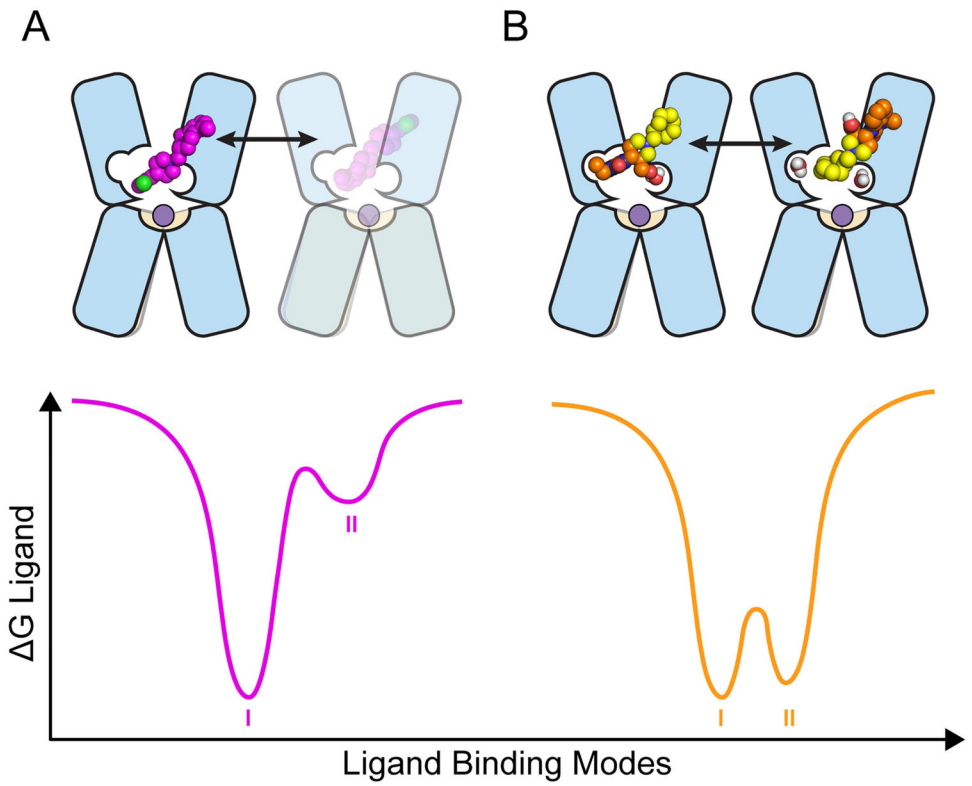

Figure 4. Potential mechanism for ligand-induced receptor stability

(**A**) High T_m ligands such as SB-612111 (purple) have a single permissible docking orientation which promotes a uniform local conformation, high receptor stability, and isolation via crystallization. (**B**) Low T_m ligands such as J-113397 (orange/yellow) have two or more binding modes with degenerate free energies, dividing the receptor population between those bound to the ligand in mode I or II, and decreasing the likelihood of isolating one receptor-ligand conformational pair via crystallization.

Table 1

Summary of Data Collection and Refinement Statistics

Data collection (APS GM/CA CAT Beamline 23ID-B/D)				
Parameters	**NOP–C-35**		**NOP–SB-612111**	
Resolution (Å)[a]	30–3.0 (3.1–3.0)		30–3.0 (3.1–3.0)	
Number of crystals	22		19	
Cell dimensions				
a, b, c (Å)	42.1, 171.7, 66.5		42.3, 168.9, 65.5	
α, β, γ (°)	90.0, 103.3, 90.0		90.0, 103.5, 90.0	
Space group	$P2_1$		$P2_1$	
Average redundancy	3.3 (3.0)		3.4 (3.3)	
Completeness (%)	90.8 (90.6)		93.2 (91.8)	
Mean I/σI	7.77 (1.18)		7.27 (1.19)	
R_{merge} (%)[b]	19.2 (n/a)		19.1 (n/a)	
R_{meas} (%)[c]	21.4 (n/a)		22.2 (n/a)	
R_{pim} (%)[d]	11.3 (85.9)		11.9 (83.7)	
unique reflections	16,902		16,552	
Refinement				
Resolution range of data used (Å)	29.63–3.00		29.85–3.00	
Reflections used	16,668		16,523	
R Factor [e]	23.5		24.0	
Free R Factor [f]	27.5		27.9	
Number of protein molecules in the asymmetric unit	2		2	
Total number of non-hydrogen atoms	A	B	A	B
Receptor	2,139	2,094	2,142	2,175
BRIL	n/a	719	n/a	710
Ligand	32	32	28	28
Lipids	23	23	60	29
Average B-factors	A	B	A	B
Receptor	83.6	82.1	65.1	63.5
BRIL	n/a	108.1	n/a	89.4
Ligand	84.2	94.9	63.4	72.9
Lipids	90.0	84.2	63.9	58.6
Overall Wilson B value ($Å^2$)	85.9		64.5	
RMSD from standard values				
Bonds (Å)	0.004		0.004	
Angles (°)	0.75		0.77	
Ramachandran plot [g]				
Residues in favored regions (%)	97.2		96.8	

Data collection (APS GM/CA CAT Beamline 23ID-B/D)		
Parameters	**NOP–C-35**	**NOP–SB-612111**
Residues in allowed regions (%)	2.8	3.2
Residues in disallowed regions (%)	0.0	0.0

[a] Values in parentheses are for the highest-resolution shell.

[b] Merging R Factor: $R_{merge} = \Sigma_h\Sigma_j|\langle I\rangle_h - I_{h,j}|/\Sigma_h\Sigma_j I_{h,j}$ where $\langle I\rangle_h$ is the mean intensity of symmetry-equivalent reflections.

[c] Redundancy-independent merging R factor: $R_{meas}=\sum_h \sqrt{\frac{n_h}{n_h-1}}\sum_j|\langle I\rangle_h - I_{h,j}|/\sum_h\sum_j I_{h,j}$ where n_h is the redundancy of structure factor h, allowing individual reflections be weighted according to their redundancy (Weiss, 2001).

[d] Precision-indicating merging R factor: $R_{pim}=\sum_h \sqrt{1/n_h-1}\sum_j|\langle I\rangle_h - I_{h,j}|/\sum_h\sum_j I_{h,j}$ describing the precision of the averaged measurement (Weiss, 2001).

[e] R factor = $\Sigma|F_{obs} - F_{calc}|/\Sigma F_{obs}$, where F_{obs} and F_{calc} are the observed and calculated structure factor amplitudes, respectively.

[f] Free R factor value was calculated as the R factor for an unrefined subset of reflection data (5% of reflections).

[g] Ramachandran plot was calculated using Molprobity (Chen et al., 2010).

Ligand electron densities are shown in detail in Figure S1.